*Forest Chemicals Review*
*www.forestchemicalsreview.com*
*ISSN: 1520-0191*
*September-October 2021 Page No. 904-921*
*Article History: Received: 22 July 2021 Revised: 16 August 2021 Accepted: 05 September 2021 Publication: 31 October 2021*

# Fusion of Infrared Polarization and Intensity Images Based on Two Dimension Variational Mode Decomposition

**Yiding Huang, Lei Zhang**
School of Mechanical and Electronic Engineering, Nanyang Normal University, Nanyang, Henan, 473061, China

***Abstract:***

This paper presents a new fusion algorithm by using infrared polarization and intensity images based on two dimensional variation mode decomposition (2D-VMD). It effectively extracts features from both infrared polarization and intensity images, and efficiently reduces information loss in the fusion process. The fusion algorithm firstly decomposes each of the two source images into a basic image and a set of intrinsic mode functions (IMF) through the 2D-VMD. These IMFs have specific directional and oscillatory characteristics and are the high frequency components of a source image. Secondly the basic image is further decomposed into a contour feature image and a texture image by using robust principal component analysis (RPCA).Thirdly the two contour feature images from the polarization basic image and intensity basic image are integrated by applying arctangent contrast modulation, the texture two images are combined based on a method, namely local average gradient summation, and then the fused basic image is obtained by the inverse transformation of RPCA. Fourthly, each high frequency component is fused by using the maximum rule. With both the fused basic image and high frequency sub-images, the final fused image is obtained by inverse transformation of 2D-VMD. The evaluation is conducted based on the comparison of the proposed fusion algorithm with other five existing fusion algorithms.

***Keywords:*** *Image fusion; Infrared polarization image; 2D-VMD; RPCA*

---

## I. INTRODUCTION

Infrared intensity imaging mainly uses thermal radiation of an object, hence an infrared intensity image describes brightness features and contour features of the object. The infrared polarization imaging exploits an object's polarization property, and the infrared polarization image mainly reflects local contrast, edge, and detailed features of the object [1]. Therefore, fusion of infrared polarization and intensity images may generate an image that can largely enhance image features of the targeted object, and significantly improves the detection rate [2], which has usages in various applications such as hide or camouflage target detection, space debris detection, underwater target detection, and public safety monitoring et al.

A great variety of fusion algorithms has been developed for the fusion of infrared polarization and intensity images. A fusion algorithm that take an average of source images pixel by pixel is simple and easy to implement, however it may lose the fused image contrasting. Although fusion algorithms based on principal component analysis (PCA) and independent component analysis (ICA) can extract main features of source images and produce a good fusion image to some extent, they tend to smooth fine features of source images, hence they are not suitable for the fusion involving infrared polarization images [3].

Multi-scale decomposition (MSD) borrows the concept of the human visual system, in which objects have different structural features in a wide scale. Thus, an image could be decomposed into a set of feature images with different scales, and the fusion of source images would be processed under the same scale between decomposed feature images. MSD may reduce information loss in image fusion processes for fine features and achieve a better fusion [4-8], such as Laplacian Pyramid decomposition [9], Wavelet analysis, Non-subsampled Contourlet Transform (NSCT), Non-subsampled Shearlet Transform (NSST), Support Vector Transform (SVT), Multi-scale Top-hat (MSTH), et al. [10].

Although the MSD fusion algorithms advance in infrared image fusion, they do have issues as mentioned in the previous studies. There are no rules for the selection of basic functions in MSD but experience, and the transformation functions are fixed for different images. However infrared polarization and intensity images are heterogeneous and describe different attributes of objects in a scene due to their different imaging mechanisms. The performance of the transformation functions varies in extracting features with regards to infrared polarization and intensity images. This leads to the loss of edges and details of an image after the transformation. Sappa, et al. evaluated qualities of fused images by combining different wavelet functions with different fusion rules. It aims to select a proper wavelet family for fusion of different images. However their method only gives a fixed combination towards the given types of images, and fails to support adaptive adjustments based on the nature of image itself. In general, one component of the source image is mixed into more than one sub-images so that components of the decomposed images may depend each other in the multi-scale transformation. It causes extracted features mixed together, and some features could be averaged away in a fusion process. It reduces the original information contained in source images. For example, Laplacian Pyramid transform produces sub-band images with high redundancy, and a heavier weight allocated to a feature weakens contributions from other features.

With respect to the issues in the multi-scale transformation in fusion of infrared polarization and intensity images, this paper proposes a fusion algorithm for infrared polarization and intensity images

Forest Chemicals Review
www.forestchemicalsreview.com
ISSN: 1520-0191
September-October 2021 Page No. 904-921
Article History: Received: 22 July 2021 Revised: 16 August 2021 Accepted: 05 September 2021 Publication: 31 October 2021

based on 2D-VM. The infrared polarization and intensity images are decomposed by using 2D-VMD, by which components of an image are independently separated and the aliasing of different features is avoided. Various fusion rules are adopted based on features extracted from the basic image and high-frequency sub-images to reduce information loss. The finally fused image is obtained by 2D-VMD inverse transformation.

The rest of the paper is organized as bellow. Section 2 introduces the transformation principle of 2D-VMD. The detailed process of the fusion algorithm is presented in Section 3. The performance evaluation and experimental results are conducted in Section 4. Section 5 is concluding.

## II. TRANSFORMATION PRINCIPLE OF 2D-VMD

2D-VMD is a new image decomposing method. The formula is as following:

$$\min_{\mu_k,\vec{\omega}_k}\left\{\sum_k\left\|\nabla\left[\mu_{AS,k}(\vec{x})e^{-j\langle\vec{\omega}_k,\vec{x}\rangle}\right]\right\|_2^2\right\} \quad s.t. \quad \sum_k \mu_k = f \tag{1}$$

Where $\vec{\omega}_k$ is the center frequency of a two dimensional signal, $\mu_{AS,k}(\vec{x})$ is the 2D analytic signal in the frequency domain after Fourier transform.

Figure 1 gives two decomposition examples. The two source images, (a1) and (a3), are decomposed by 2D-VMD, results in (b1)-(e1) and (b3)-(e3), and NSST, results in (a2)-(e2) and (a4)-(e4), respectively. From the 2D-VMD results, it can be seen that the source images are decomposed into a basic image with frequency consistency and high-frequency sub-images of independent components (IMF components). Note that these high-frequency sub-images have specific directional and oscillatory characteristics, meanwhile, there is less redundancy among them. Hence, the high frequency sub-images shown in Fig. 1 (c1) - (e1) contain ellipses with different direction and frequency in the source image. Furthermore, independent features in the second source image are adaptively extracted, as shown in Fig. 1 (c3) - (e3) in which each high frequency sub-image only represents features with the same frequency and a direction in the source image, but the basic image preferably contains components of frequency consistency with the source image. However for the NSST results, features of the source image are mixed in high frequency components, there is a heavy redundancy among them, and they are dependent each other (poor independence) so that the aliasing of features is obvious. For the first source image, elliptic features appear in each high frequency sub-image in different directions as shown in in Fig. 1 (d2) - (e2); whilst for the second source image, the aliasing is terribly appeared in Fig. 1 (b4) - (e4). These indicate that 2D-VMD is superior to NSST in feature independency when decomposing an image. The independency is an important characteristic to ensure less information loss in the image fusion process,

Forest Chemicals Review
www.forestchemicalsreview.com
ISSN: 1520-0191
September-October 2021 Page No. 904-921
Article History: Received: 22 July 2021 Revised: 16 August 2021 Accepted: 05 September 2021 Publication: 31 October 2021

which is described in Section 3.

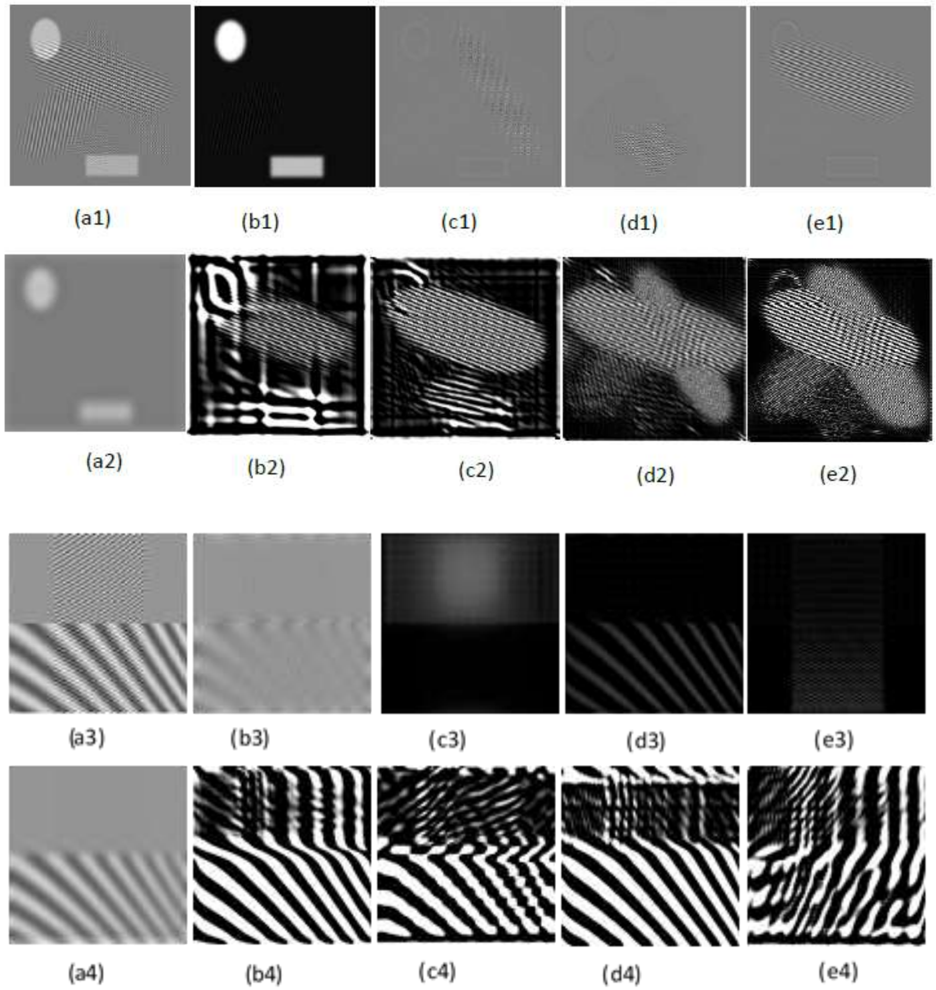


Fig 1: The decomposition diagram of 2D-VMD and NSST, (a1) and (a3) are input images, (b1) and (b3) are basic images of 2D-VMD, (c1) - (e1) and (c3) - (e3) are high frequency sub-images of 2D-VMD, (a2) and (a4) are low frequency images of NSST, (b2) - (e2) and (b4) - (e4) are high frequency images of NSST

## III. THE FUSION ALGORITHM

As discussed in Section 2, an image can be adaptively decomposed into a basic image and a few high frequency sub-images. The basic image contains the basic information of the source image, and the high frequency sub-images reflect the high frequency components with different frequency bands of the source image. A fusion algorithm based on 2D-VMD, as shown in Figure 2, is proposed to extract useful information from source images to improve image quality and enrich information carried in a fused

Forest Chemicals Review
www.forestchemicalsreview.com
ISSN: 1520-0191
September-October 2021 Page No. 904-921
Article History: Received: 22 July 2021 Revised: 16 August 2021 Accepted: 05 September 2021 Publication: 31 October 2021

image.

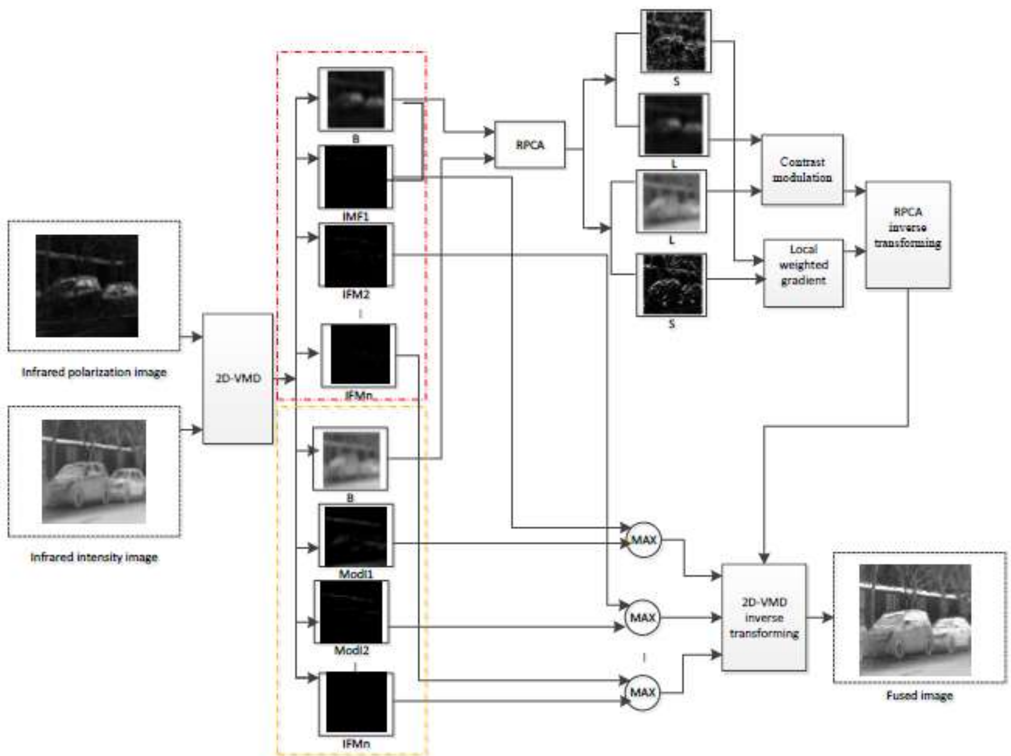


Fig 2: The flow chart of the proposed algorithm, B is the basic image, IFM is the intrinsic mode functions, L is the low-rank image, S is the sparse image

### 3.1 The Fusion Rule to 2D-VMD Basic Images

The current fusion rules of MSD mainly adopt energy weighting or weighted average of low frequency sub-images from relevant source images. However they are less effective in fusing contrast and texture features in low frequency sub-images. The analysis in Section 2 has indicated that the basic image of 2D-VMD contains contour features and small texture features. The energy weighting or weighted average in fusion may degrade the image contrast and cause the texture loss. To tackle these issues, it is proposed to separate contour features and small texture features in the basic image, and then fusion processes are applied to the two features separately.

The robust principal component analysis (RPCA) is a method sparsely representing an image [11]. By using the RPCA, an image can be represented as the superposition of a low-rank matrix *L* and a

Forest Chemicals Review
www.forestchemicalsreview.com
ISSN: 1520-0191
September-October 2021 Page No. 904-921
Article History: Received: 22 July 2021 Revised: 16 August 2021 Accepted: 05 September 2021 Publication: 31 October 2021

sparse matrix $S$. $L$ contains similar features of and is redundant to the original image, and $S$ describes fine features of the original image [12-14]. The formula is expressed as below:

$$H = L + S \tag{2}$$

Where H is an input image, $L$ is the low-rank image, $S$ is the sparse image. The decomposing process is as follows:

$$\min_{L.S} \|L\|_* + \lambda \|S\|_1 \qquad s.t. H = L + S \tag{3}$$

Where $\|\bullet\|_*$ denotes the nuclear norm of a matrix, $\|\bullet\|_1$ represents the $L_1$-norm, and $\lambda$ is a controlling parameter.

In practice, the RPCA well separate the similar features (contour and strong local contrast region) and the small texture features in the two basic images induced from the infrared polarization and intensity images. Different fusion rules are applied to these features.

3.1.1 The fusion rule for L images

Due to different imaging mechanisms, pixel values of an infrared polarization image are usually lower than those of an infrared intensity image, and pixel values from a strong contrast region are also lower than those of the infrared intensity image. Meanwhile, contour features of $L$ overlap with contrast features in the basic image of the infrared intensity image, and the scene with obvious contour features shows a strong contrast between the background and an object. For better fusing contrast features of the infrared polarization and intensity images, firstly, a image contrasting is defined by the ratio between pixel values of an image and the mean value of the image, as in formula (4).

$$C_n(i, j) = L_n(i, j) / \bar{L}_n \tag{4}$$

Where $C_n$ is the image contrasting, $L_n(i, j)$ is the pixel value at coordinate ($i$, $j$), $\bar{L}_n$ is the mean value of an image, $n \in I$ or $P$.

The range of $C_n$ values could be large. This may lead to overflow in image regions where the contrast is strong when directly applying weights to $C_n$. For better combining contrast features from the two source images, the method introduced by Piella is adopted as in equation (5).

Forest Chemicals Review
www.forestchemicalsreview.com
ISSN: 1520-0191
September-October 2021 Page No. 904-921
Article History: Received: 22 July 2021 Revised: 16 August 2021 Accepted: 05 September 2021 Publication: 31 October 2021

$$J(r) = k\,acr\,tan(r) \tag{5}$$

$J(r)$, a sigmoid-like function, behaves nonlinearly. It increases the contrast for small differences $|r|$ while saturates for larger $|r|$. Changing the $r$ of the function tunes the final contrast: the larger the $r$, the greater the contrast.

The $J(r)$ function is effective in de-noising and smoothing and it is normalized transformation curve. Therefore $C_n$ is normalized by using a tangent function, the formula is as below:

$$w_n^C(i,j) = acr\,tan(C_n(i,j))/(\pi/2) \tag{6}$$

The fused result of $L$ is expressed in equation (7)

$$F_C(i,j) = w_I^C(i,j) * L_I(i,j) + w_P^C(i,j) * L_P \tag{7}$$

Where $F_C$ is the fused image of the two L images, $w_n^C$ for $n \in L \text{ or } P$ are weights.

3.1.2 The fusion rule for $S$ images

The sparse image mainly describes fine texture features of the basic image and also reflects variation between neighbor pixels. The average gradient defines variations of neighbor pixels in an image both horizontally and vertically. The local average gradient sum is expressed in formula (8).

$$avegrad_n(i,j) = \sqrt{\left(\frac{1}{M-1} \times \frac{1}{N-1}\right) \sum_{i=1}^{M-1} \sum_{j=-1}^{N-1} \frac{\left(|S_n(i,j) - S_n(i+1,j)|^2 + |S_n(i,j) - S_n(i,j+1)|^2\right)}{2}} \tag{8}$$

The local average gradient sum *avegrad* in formula (13) is used to construct weights of $S$ images in fusion. $M \times N$ is the size of a sliding window. In the practice, M = N = 3. The result of fusion is as follows:

$$F_S(i,j) = w_I^S(i,j) * S_I(i,j) + w_P^S(i,j) * S_P(i,j) \tag{9}$$

$$w_I^S(i,j) = \frac{avegrad_I(i,j)}{avegrad_I(i,j) + avegrad_P(i,j)} \tag{10}$$

Forest Chemicals Review
www.forestchemicalsreview.com
ISSN: 1520-0191
September-October 2021 Page No. 904-921
Article History: Received: 22 July 2021 Revised: 16 August 2021 Accepted: 05 September 2021 Publication: 31 October 2021

$$w_P^S(i,j) = \frac{avegrad_P(i,j)}{avegrad_I(i,j) + avegrad_P(i,j)} \tag{11}$$

Where $F_S$ is fused image of sparse images, $w_n^S$ is fusion weighting of sparse images, *avegrad* is the local average gradient sum.

Finally, the fused image from the infrared polarization and intensity basic images ($F_H$) is obtained.

$$F_H = F_C + F_S \tag{12}$$

3.2 The Fusion Rule of High Frequency Sub-Images of 2D-VMD

Infrared polarization and intensity images describe polarization and radiation characteristics of a scene, respectively. In general, an infrared polarization image reflects high frequency features of a scene, whilst an infrared intensity image reflects low frequency features of a scene. Therefore they are complementary in describing a scene in terms of frequency of the scene. After infrared polarization and intensity images are decomposed by 2D-VMD, as described in Section 2, high frequency sub-images are independent each other, and each of them reflects unique features of a source image. Between the polarization image and the intensity image, the higher value towards a pixel is always selected in fusion to recover image information in all frequency bands of a scene. Hence, the maximum fusion rule is applied as expressed below.

$$F_{IFM_n} = \begin{cases} I_{IFM_n} & if \left| I_{IFM_n} \right| \geq \left| P_{IFM_n} \right| \\ P_{IFM_n} & else \end{cases} \tag{13}$$

Where $F_{IMF_n}$ is fused results of different frequency band sub-images, $I_{IFM_n}$ and $P_{IFM_n}$ are high frequency feature images of infrared polarization and intensity images, respectively. Depending on the number of high frequency sub-images, n=1, 2, 3, 4……. In practice, we choose n=3 or 4 in decomposition. This means there are three or four high frequency sub-images after decomposition.

The final fused image *F* is obtained by an inverse transform of the 2D-VMD in equation (14).

$$F = 2D - VMD^{-1}(F_H, F_{IFM_n}) \tag{14}$$

Where $F_H$ and $F_{IFM_n}$ are the fused images by the basic images and high frequency sub-images, respectively.

*Forest Chemicals Review*
*www.forestchemicalsreview.com*
*ISSN: 1520-0191*
*September-October 2021 Page No. 904-921*
*Article History: Received: 22 July 2021 Revised: 16 August 2021 Accepted: 05 September 2021 Publication: 31 October 2021*

## IV. ANALYSIS WITH THE EXPERIMENTAL RESULTS

To show the advantages of the proposed fusion algorithm, NSST, SVT-TopHat, NSST-PCA [15], NSCT-PCNN [16], and NSCT-SR [17] are compared with the proposed fusion algorithm. Six pairs of source images used in the experiment are presented in Figure 3 as I1-I6 (infrared intensity images) and P1-P6 (infrared polarization images), and the final fused images are demonstrated in Figure 4.

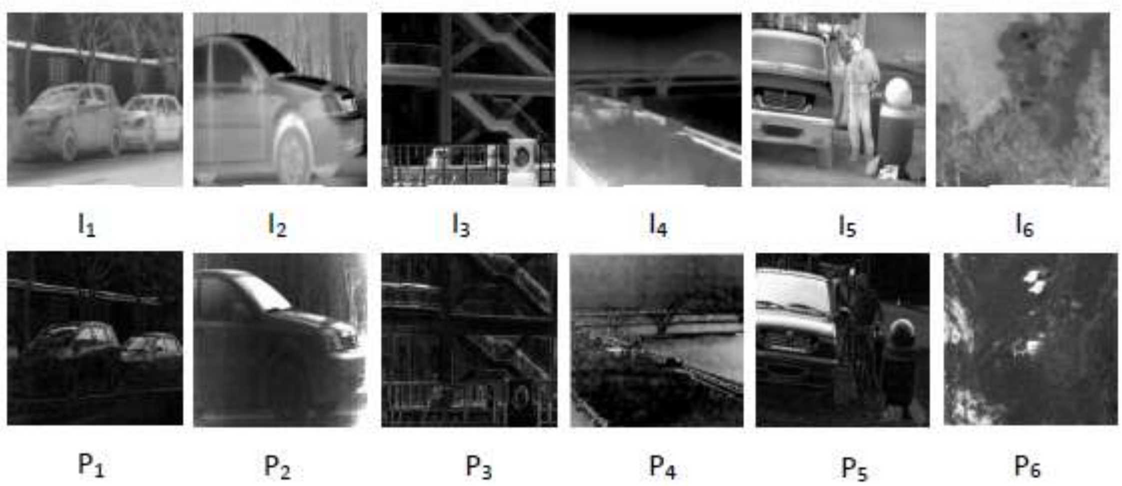


Fig. 3: Source images: I1-I6 intensity images; P1-P6 polarization images

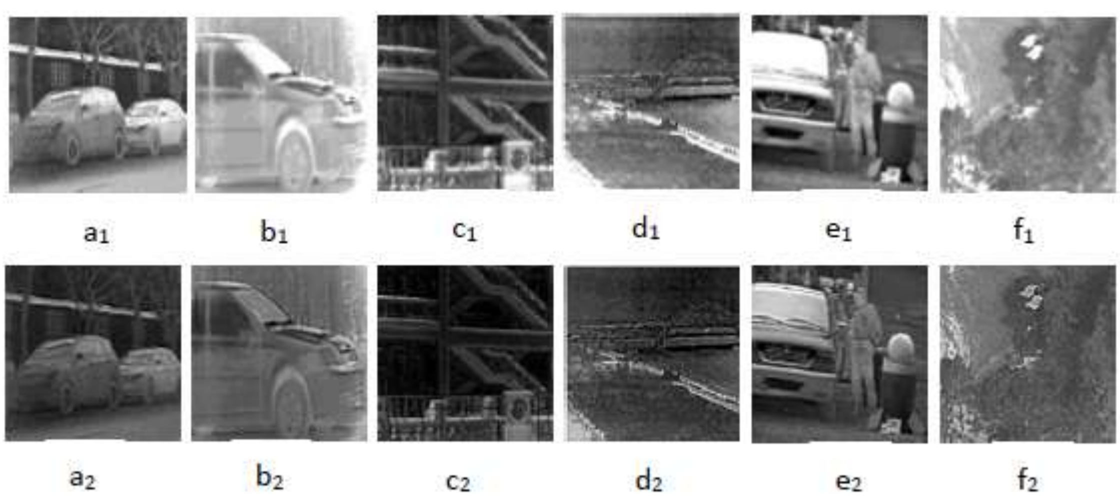

*Forest Chemicals Review*
*www.forestchemicalsreview.com*
*ISSN: 1520-0191*
*September-October 2021 Page No. 904-921*
*Article History: Received: 22 July 2021 Revised: 16 August 2021 Accepted: 05 September 2021 Publication: 31 October 2021*

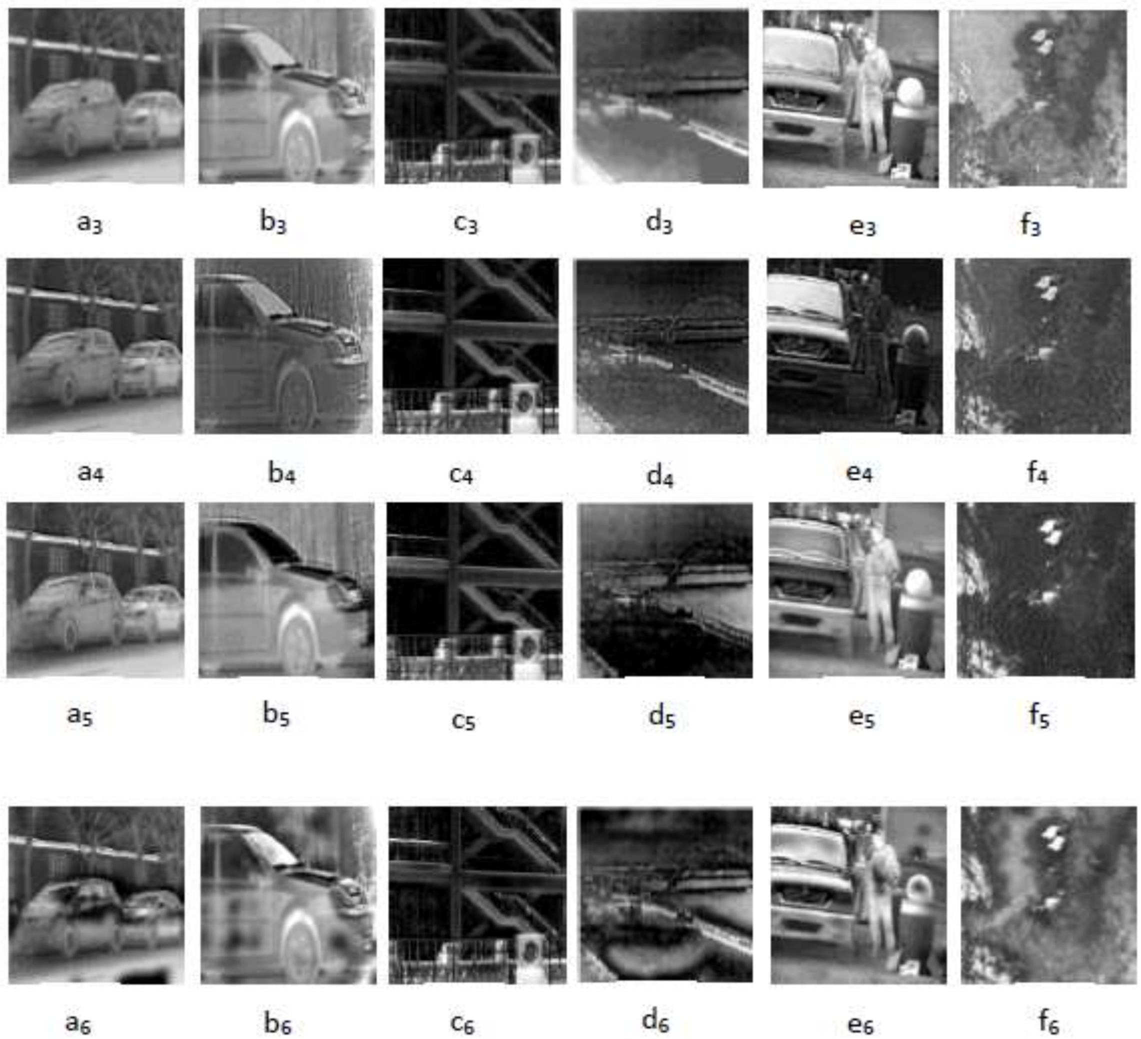


Fig 4: Fused images ($a_1$) - ($f_1$) from the proposed method, ($a_2$) - ($f_2$) from NSST, ($a_3$) - ($f_3$) from SVT-Tophat, ($a_4$) - ($f_4$) from NSST-PCA, ($a_5$) - ($f_5$) from NSST-PCNN, ($a_6$) - ($f_6$) from NSCT-SR

## 4.1 Comparison of Fused Results

We can see from the fused images in Fig. 4 that the proposed method better preserves the brightness feature of the infrared intensity image. For example, the overall brightness or visual effect of images in Fig.4 ($a_1$) - ($f_1$) is better than those fused images from other methods. The brightness difference feature transfer ability of other fusion methods is poor, especially, when the image changes, the performance is more obvious. For example, the fused results from NSST-PCA are dark as a whole, as shown in Fig. 4 ($a_4$) - ($f_4$); and the fused results from NSCT-SR, shown in Fig. 4 ($a_6$) - ($f_6$) exist errors in bright/dark

*Forest Chemicals Review*
*www.forestchemicalsreview.com*
*ISSN: 1520-0191*
*September-October 2021 Page No. 904-921*
*Article History: Received: 22 July 2021 Revised: 16 August 2021 Accepted: 05 September 2021 Publication: 31 October 2021*

regions, which is mainly due to the great difference of pixel values between infrared polarization and intensity images, and the fine texture features of low frequency sub-images are extracted using SR after a multi-scale transform, which ignores the region consistency feature in both types of images.

The proposed method better transfers the contrast feature of the infrared polarization image and preserves regions with high local contrast in it. For example, the strong contrast features are remained in the infrared polarization images as cars' windows (Figs. 4 (a1) - (b1)) and buildings (Fig. 4 (a3)). Nevertheless the contrast features are partially degraded in the fused images from other fusion algorithms. This can be seen from the regions of cars' front windows in Figs. 4 ($a_1$) and (e1), and the water surface in Fig. 4 (d1). The fused images in Figs. 4 ($a_2$) - ($a_5$), ($d_2$), ($d_4$) and ($e_2$) - ($e_6$) do not perverse the strong contrast features of cars front windows and the water surface in the infrared polarization images. The proposed method preserves detailed difference features between infrared polarization and intensity images, and shows superior to other algorithms in image clarity and edge feature of car (Figs. 4(a1)-(b1), tree (Figs. 4(a1-f1)), door (Figs. 4(c1)), wall (Figs. 4(c1)) and bridge (Figs. 4 (d1)). 2D-VMD outperforms the other fusion algorithms in retaining image texture features. This can be seen from the comparison of the fused image in Fig. 4 (c1) to those images in Fig.4. ($c_2$) - ($c_6$) for the edge of guardrail and staircase, and the texture of the building. The texture of trees in Fig. 4 (a1) - (a6) also shows the advantage of 2D-VMD in better preserving image texture features.

4.2 Objective Evaluation of the Fused Images

Objective evaluation of the fused images are based on five indexes, Spatial Frequency (SF), Standard Deviation (STD), Edge Strength (QF), the Mean of an image, and information index $R_{ab/f}$ [17].

1) The spatial frequency (SF) describes variance of image pixel values in horizontal and vertical. It reflects image clarity: the greater the value of SF show the image is the better clarity. The formula is as follows:

$$SF = \sqrt{RF^2 + CF^2} \tag{15}$$

Where RF and CF are defined as follows:

$$RF = \sqrt{\frac{\sum_{x=1}^{M}\sum_{y=1}^{N}(F(x,y) - F(x,y-1))}{M \times N}} \tag{16}$$

Forest Chemicals Review
www.forestchemicalsreview.com
ISSN: 1520-0191
September-October 2021 Page No. 904-921
Article History: Received: 22 July 2021 Revised: 16 August 2021 Accepted: 05 September 2021 Publication: 31 October 2021

$$CF = \sqrt{\frac{\sum_{x=1}^{M}\sum_{y=1}^{N}(F(x,y)-F(x-1,y))}{M \times N}} \tag{17}$$

2) The standard deviation (STD) indicates the contrast feature of an image. The greater the STD value is, the image contrasting is better.

3) The edge strength (QF) depicts the edge feature. The high value of the QF show that the edge fusion effect is well. The formulas is as follows:

$$QF = \sum_{i=1}^{M}\sum_{j=1}^{N} GF(i,j) \tag{18}$$

Where *GF* is defined as:

$$GF(i,j) = \sqrt{s_F^x(i,j)^2 + s_F^y(i,j)^2} \tag{19}$$

Where $S_F^x(i,j)^2$ and $S_F^y(i,j)^2$ indicate the Sobel operator convoluting image *F* horizontally and vertically, respectively.

4) The MEAN of an image describes the brightness of an image. The higher the value is, the brighter is the image.

5) The $R_{ab/f}$ indicates the amount of information contributing from each of the source images to the fused image. The similarity between the fused image and source image is large that the value of R is large. The formulas are as follows:

$$r(D_k, S_k) = \frac{\sum_i \sum_j ((D(i,j)-\overline{D})*(S_k(i,j)-\overline{S_k}))}{\sqrt{\sum_i \sum_j (D\,(i,j)-\overline{D})^2 + \sum_i \sum_j (S_k(i,j)-\overline{S_k})^2}} \tag{20}$$

$$R_{ab/f} = r(I,F) + r(P,F) \tag{21}$$

$S_k$ is the source images, and $k \in I$ or $P$ in this study. In addition, $\overline{D}$ and $\overline{S_k}$ are the mean value of D and $S_k$, respectively. Moreover, $R_{ab/f}$ is the sum of the correlation of the differences.

*Forest Chemicals Review*
*www.forestchemicalsreview.com*
*ISSN: 1520-0191*
*September-October 2021 Page No. 904-921*
*Article History: Received: 22 July 2021 Revised: 16 August 2021 Accepted: 05 September 2021 Publication: 31 October 2021*

**Table I. $P_1$ and $I_1$ fused image evaluation indexes**

| **Fusion algorithms** | **SF** | **STD** | **QF** | **MEAN** | **$R_{ab/f}$** |
|---|---|---|---|---|---|
| 2D-VMD | **21.4475** | **51.3358** | **79.9902** | **116.1883** | **1.9218** |
| NSST | 17.9967 | 31.6117 | 66.5478 | 69.8718 | 1.3959 |
| Svt-top hat | 13.3472 | 43.5733 | 74.0416 | 110.2721 | 1.5522 |
| NSST-PCA | 18.6006 | 42.0533 | 74.0416 | 101.1889 | 1.4619 |
| NSST-PCNN | 18.4161 | 45.8973 | 74.1572 | 113.2356 | 1.3705 |
| NSCT-SR | 17.9080 | 45.8175 | 73.7168 | 97.0517 | 0.7717 |

**Table II. $P_2$ and $I_2$ fused image evaluation indexes**

| **Fusion algorithms** | **SF** | **STD** | **QF** | **MEAN** | **$R_{ab/f}$** |
|---|---|---|---|---|---|
| 2D-VMD | **21.3748** | **48.5547** | **86.2638** | **183.3426** | **1.9146** |
| NSST | 17.1286 | 28.3996 | 67.8597 | 103.4040 | 1.7990 |
| Svt-top hat | 15.2129 | 35.2230 | 62.9558 | 140.0257 | 1.7107 |
| NSST-PCA | 17.5181 | 33.2529 | 69.5848 | 97.7891 | 1.8106 |
| NSST-PCNN | 17.5978 | 45.5877 | 73.6781 | 128.7341 | 1.1292 |
| NSCT-SR | 17.8993 | 47.3743 | 77.1269 | 127.1802 | 1.5399 |

**Table III. $P_3$ and $I_3$ fused image evaluation indexes**

| **Fusion algorithms** | **SF** | **STD** | **QF** | **MEAN** | **$R_{ab/f}$** |
|---|---|---|---|---|---|
| 2D-VMD | **33.0005** | **53.2310** | **123.2716** | **85.8591** | **1.8603** |
| NSST | 30.0911 | 36.6841 | 112.5722 | 41.4257 | 1.5420 |
| Svt-top hat | 27.6231 | 47.2630 | 100.6536 | 59.5025 | 1.7130 |
| NSST-PCA | 30.8979 | 52.6549 | 119.8145 | 50.3100 | 1.6592 |
| NSST-PCNN | 30.5084 | 52.9646 | 117.2793 | 50.9014 | 1.6346 |
| NSCT-SR | 28.9403 | 51.1502 | 113.0281 | 53.2451 | 1.6243 |

Forest Chemicals Review
www.forestchemicalsreview.com
ISSN: 1520-0191
September-October 2021 Page No. 904-921
Article History: Received: 22 July 2021 Revised: 16 August 2021 Accepted: 05 September 2021 Publication: 31 October 2021

**Table IV. $P_4$ and $I_4$ fused image evaluation indexes**

| Fusion algorithms | SF | STD | QF | MEAN | $R_{ab/f}$ |
|---|---|---|---|---|---|
| 2D-VMD | **25.4904** | **55.8067** | **95.2436** | **120.3002** | **1.9035** |
| NSST | 25.0894 | 37.6762 | 82.3774 | 68.8672 | 1.6912 |
| Svt-top hat | 16.4919 | 46.0371 | 56.8541 | 100.8366 | 1.6150 |
| NSST-PCA | 25.4452 | 43.6882 | 84.2898 | 70.9128 | 1.7042 |
| NSST-PCNN | 25.3986 | 50.2934 | 85.9878 | 62.5136 | 1.0370 |
| NSCT-SR | 25.1403 | 49.6842 | 90.0522 | 70.4472 | 1.3666 |

**Table V. $P_5$ and $I_5$ fused image evaluation indexes**

| Fusion algorithms | SF | STD | QF | MEAN | $R_{ab/f}$ |
|---|---|---|---|---|---|
| 2D-VMD | **30.8399** | **80.7054** | **113.2584** | 131.2039 | **1.9414** |
| NSST | 30.1087 | 50.6454 | 104.1522 | 90.8839 | 1.3977 |
| Svt-top hat | 23.8406 | 57.7209 | 90.7554 | **133.6840** | 1.4924 |
| NSST-PCA | 30.4038 | 64.0356 | 105.1463 | 64.2101 | 1.4100 |
| NSST-PCNN | 30.5871 | 55.1791 | 111.5507 | 128.3984 | 0.8634 |
| NSCT-SR | 29.6062 | 58.3115 | 111.0028 | 126.0203 | 1.1354 |

**Table VI. $P_6$ and $I_6$ fused image evaluation indexes**

| Fusion algorithms | SF | STD | QF | MEAN | $R_{ab/f}$ |
|---|---|---|---|---|---|
| 2D-VMD | **19.7130** | **41.8796** | **80.1109** | **145.6673** | **1.9518** |
| NSST | 18.6225 | 26.9311 | 75.8559 | 100.3246 | 1.5347 |
| Svt-top hat | 12.5918 | 34.6554 | 59.3788 | 133.6840 | 1.5848 |
| NSST-PCA | 19.0275 | 30.5386 | 77.1554 | 88.8756 | 1.5312 |
| NSST-PCNN | 19.0758 | 36.9741 | 76.2856 | 75.8962 | 1.0534 |
| NSCT-SR | 18.8968 | 36.8702 | 79.7526 | 113.6354 | 0.9819 |

Tables I-VI demonstrate that the SF, STD, and QF values of this paper fusion images are the highest. As shown in Table V, the MEAN value obtained by SVT-Tophat has the highest value. This reveals the fact that SVT-Tophat puts extra efforts towards the fusion between brightness and dark features of two

*Forest Chemicals Review*
*www.forestchemicalsreview.com*
*ISSN: 1520-0191*
*September-October 2021 Page No. 904-921*
*Article History: Received: 22 July 2021 Revised: 16 August 2021 Accepted: 05 September 2021 Publication: 31 October 2021*

images. This may cause excessive luminance in some areas in this specific image (image 5).Otherwise, the MEAN values presented in other tables indicate the highest MEAN of the fused image is from 2D-VMD, which fuses the brightness features of source images effectively. The $R_{ab/f}$ of this paper fusion algorithm is the largest, which show that the similarity between fused image and source image is the highest, and the proposed fusion algorithm has the best ability to transfer the complementary features between the source images.

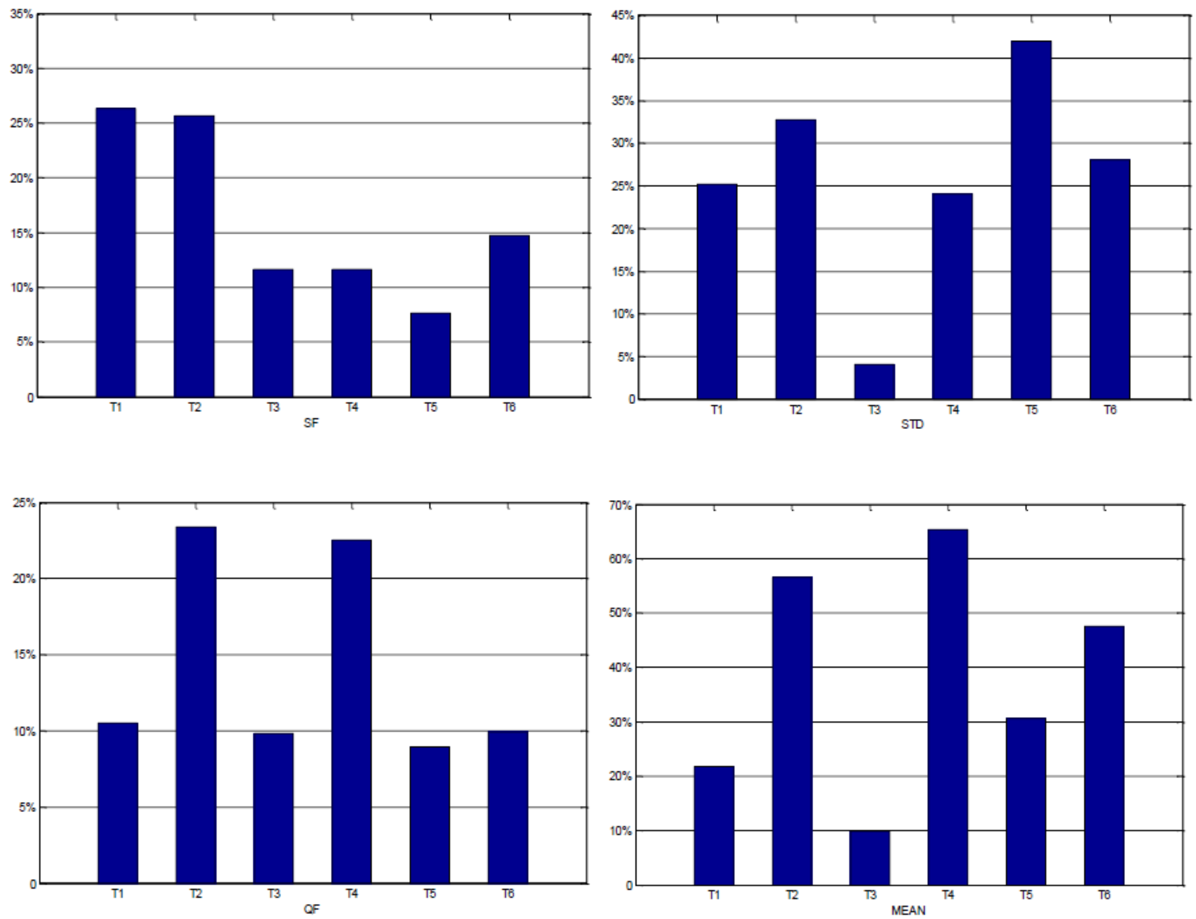

*Forest Chemicals Review*
*www.forestchemicalsreview.com*
*ISSN: 1520-0191*
*September-October 2021 Page No. 904-921*
*Article History: Received: 22 July 2021 Revised: 16 August 2021 Accepted: 05 September 2021 Publication: 31 October 2021*

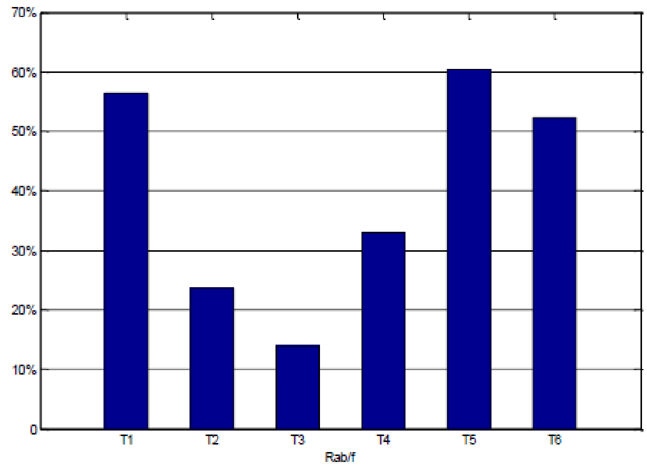


Fig 5: The average improvement of the proposed method over the five evaluation indexes

Fig. 5 presents the average improvement percentage over the five evaluation indexes based on the comparison between the proposed method and the other fusion algorithms for the six testing images. The average improvement percentage (A.I.P) is calculated by equation (23)

$$\text{A.I.P} = \frac{1}{n}\sum_{x=1}^{n}\frac{Y_{2D-VMD} - Y_x}{Y_x} \tag{22}$$

Where n is the number of the other fusion methods involved in the comparison, here it is 5; x depicts the other fusion methods; and Y represents evaluation index, i.e. *SF*, *STD*, *QF*, *MEAN*, and $R_{ab/f}$ .

It demonstrates that the index of image fusion obtained by using the proposed method has obvious advantages over other algorithms for the six tested images. This shows that this paper algorithm well fuses structure and fine texture features from infrared polarization and intensity images and observably improves the quality of the fused image.

The subjective and objective evaluations show that the method proposed by this paper can deceptively extract and fuse the different kinds of image features from infrared polarization and intensity images, and the fusion algorithm of this paper improve the image clarity and visual effect very well.

*Forest Chemicals Review*
*www.forestchemicalsreview.com*
*ISSN: 1520-0191*
*September-October 2021 Page No. 904-921*
*Article History: Received: 22 July 2021 Revised: 16 August 2021 Accepted: 05 September 2021 Publication: 31 October 2021*

## V. CONCLUSION

This paper presents a novel fusion algorithm to effectively extract useful information from both infrared polarization and intensity images under multi-scale decomposition based on the principle of 2D-VMD. The proposed fusion method subtly exploits characteristics of the basic image and the set of high frequency sub-images after 2D-VMD, and developed efficient fusion rules with respects to different features. It significantly improves the quality of fused images in terms of preserving fine texture features and adjusting brightness changes over source images. The main contributions can be summarized as below.

(1) The 2D-VMD is employed in image decomposition with the purpose of information fusion for infrared polarization and intensity images. The characteristics of 2D-VMD adaptively separates high frequency features of an image at different frequency bands. Each feature represents independent components of the source images. Due to its adaptability, this property applies to various infrared polarization and intensity images. It has been proved in our experiments. Because of the clear separation of high frequency features, it made it possible to develop effective fusion rules with respect to different features for a better fusion.

(2) The RPCA is applied to transform the basic image into two images, L for similar features and S for fine texture features of the original image. Individual fusion rules, the arctangent transformation and local average gradient sum, are developed for fusing L images and S images, respectively. This ensures that the fine texture features and contrast features contained in the infrared polarization and intensity basic images are well preserved and this also reduces the information loss in the fused image.

The experiment results show that this paper fusion algorithm can well combine the structure. The evaluation indexes of the proposed fusion algorithm is the best.

## REFERENCES

[1] Niu T, Yang F B, Wang X X, et al. Establishment of set-valued mapping between difference characteristics and fusion algorithms. *Infrared and Laser Engineering*. 2015, 44(3):1073-1079.
[2] Liang J, Zhang W, Ren L, et al. Polarimetric dehazing method for visibility improvement based on visible and infrared image fusion. *Applied Optics*, 2016, 55(29):8221-8226.
[3] Bai X and Zhang Y. Detail preserved fusion of infrared and visual images by using opening and closing based toggle operator. *Optics & Laser Technology*, 2014, 63(63):105-113.
[4] Li S, Kang X, Fang L, et al. Pixel-level image fusion: A survey of the state of the art. *Information Fusion*, 2017, 33:100-112.
[5] Du J, Li W, Lu K, et al. An overview of multi-modal medical image fusion. *Neurocomputing*, 2016, 215:3-20.
[6] Li H, Qiu H, Yu Z, et al. Multifocus image fusion via fixed window technique of multiscale images and non-local

*Forest Chemicals Review*
*www.forestchemicalsreview.com*
*ISSN: 1520-0191*
*September-October 2021 Page No. 904-921*
*Article History: Received: 22 July 2021 Revised: 16 August 2021 Accepted: 05 September 2021 Publication: 31 October 2021*

means filtering. *Signal Processing*, 2017, 138:71-85.

[7] He K, and Wang Q. Infrared and visible image fusion based on target extraction in the nonsubsampled contourlet transform domain. *Journal of Applied Remote Sensing*, 2017, 11(1):015011.

[8] Zhang Q, and Maldague X. Multisensor image fusion approach utilizing hybrid pre-enhancement and double nonsubsampled contourlet transform. *Journal of Electronic Imaging*, 2017, 26(1):010501.

[9] Yue Z, and Li F M. An infrared polarization image fusion algorithm based on oriented Laplacian pyramid. *Selected Papers From Conferences of the Photoelectronic Technology Committee of the Chinese Society of Astronautics: Optical Imaging, Remote Sensing, and Laser-Matter Interaction. International Society for Optics and Photonics*, 2014:914208-914208-11.

[10] Ibrahim R, Alirezaie J, and Babyn P. Pixel level jointed sparse representation with RPCA image fusion algorithm. *International Conference on Telecommunications and Signal Processing. IEEE*, 2015:592-595.

[11] Fu Z, Wang X, Xu J, et al. Infrared and visible images fusion based on RPCA and NSCT. *Infrared Physics & Technology*, 2016, 77:114-123.

[12] Zhang B, Lu X, Pei H, et al. Multi-focus image fusion based on sparse decomposition and background detection. *Digital Signal Processing*, 2016, 58:50-63.

[13] Dang C, and Radha H. RPCA-KFE: Key Frame Extraction for Consumer Video based Robust Principal Component Analysis. *IEEE Transactions on Image Processing*, 2014, 24(11):3742-3753.

[14] Piella G. Image Fusion for Enhanced Visualization: A Variational Approach. *Int J Comput Vis*, 2009, 83: 1–11.

[15] Miao Q, and Wang B. A novel image fusion method using WBCT and PCA. *Chinese Optics Letters*, 2008, 6(2):104-107.

[16] Qu X B, Yan J W, and Xiao H Z. Image Fusion Algorithm Based on Spatial Frequency-Motivated Pulse Coupled Neural Networks in Nonsubsampled Contourlet Transform Domain. *Acta Automatica Sinica*, 2008, 34(12):1508-151.

[17] Zhang X L, Li X F, and Li J. Validation and Correlation Analysis of Metrics for Evaluating Performance of Image Fusion. *ACTA AUTOMATICA SINICA*, 2014, 40(2):306-315.